Electron gas and dense hydrogen:
From ground state energies to phase diagrams

Markus Holzmann
LPMMC, CNRS UGA Grenoble

- Ground state energies:
  iterated backflow, neural network wave functions

- Energy gaps (insulators):
  single particle excitations (charged gap)
  particle-hole excitations (neutral gap)

- Fermi liquid properties (metals):
  momentum distribution
  renormalization factor Z
  effective mass m*

Plasmas in condensed matter (I)

“Condensed” matter:

- (non-relativistic) Hamiltonian for ions and electrons (Coulomb interaction)

$$H = -\sum_n \frac{\hbar^2 \nabla_n^2}{2M} - \sum_i \frac{\hbar^2 \nabla_i^2}{2m} + \sum_{n<m} \frac{e^2}{|\mathbf{r}_i - \mathbf{r}_j|} - \sum_{n,i} \frac{Ze^2}{|\mathbf{r}_i - \mathbf{R}_n|} + \sum_{n<m} \frac{Z^2 e^2}{|\mathbf{R}_n - \mathbf{R}_m|}$$

$$= -\sum_n \frac{\hbar^2 \nabla_n^2}{2M} + H_e(\mathbf{R})$$

- Temperatures much smaller than electronic Fermi temperature $T \ll T_F$
  Energetics: Born-Oppenheimer approximations (electronic ground state for fixed/static ions)

$$H_e(\mathbf{R})\Psi(\mathbf{r}) = E_0(\mathbf{R})\Psi(\mathbf{r})$$

“Plasma” physics:

- “collective” electronic phases (not bandstructure): electron gas (one component plasma)
- “collective” nuclear effects at low temperature: quantum liquids, ultracold atoms,…
- “emergent” phases of long living excitations (quasi-particles): excitons,…

Plasma in condensed matter (II)

Electronic matter:

- (High Tc) supraconductors…:
  - Hubbard model(s) (phase diagram)
  - Phases of continuum models (electron gas)
  - “ab-inito” description of materials from electronic structure: embedding, downfolding...

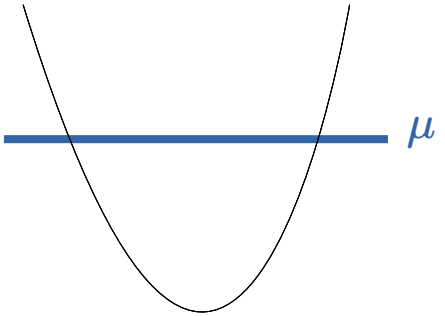

- Excitation spectra and many-body correlations:
  - Fermi liquid vs Mott
  - Photon absorption
  - Excitonic effects, plasmons...
  - (Shiwei Zhang, David Ceperley, Ilya Esterlis, Yubo Yang, Carlos Sa de Melo, David Linteau)

Semiconductor excitons:

- composite bosons with dominant dipolar interaction, nanostructures...
  - Bose condensation, e-h plasma: bi-excitons, qudri-excitons… (David Neilson, Filippo Pascucci, Stefania de Palo, ...)

Ultracold atoms, helium liquids:

- effective short-range interactions (few parameters, quantitatively measured)

Phase diagram of the homogeneous electron gas: an ideal problem for computational methods!

Electron gas: (jellium, HEG,OCP)

$$H = -\frac{\hbar^2}{2m_e}\sum_i \nabla_i^2 + \sum_{i<j}\frac{e^2}{|\mathbf{r}_i - \mathbf{r}_j|}$$

Quantum Monte Carlo methods:

- Based on variational principle

$$E_0(N) \le E_T(N) \equiv \frac{\langle \Psi_T | H | \Psi_T \rangle}{\langle \Psi_T | \Psi_T \rangle}$$

- Explicitly correlated wave functions (Slater-Jastrow,…)
- Stochastical improvements
- Monte Carlo integrations
- finite number of particles N

VOLUME 45, NUMBER 7 PHYSICAL REVIEW LETTERS 18 AUGUST 1980

Ground State of the Electron Gas by a Stochastic Method

D. M. Ceperley
National Resource for Computation in Chemistry, Lawrence Berkeley Laboratory, Berkeley, California 94720
and
B. J. Alder
Lawrence Livermore Laboratory, University of California, Livermore, California 94550
(Received 16 April 1980)

An exact stochastic simulation of the Schroedinger equation for charged bosons and fermions has been used to calculate the correlation energies, to locate the transitions to their respective crystal phases at zero temperature within 10%, and to establish the stability at intermediate densities of a ferromagnetic fluid of electrons.

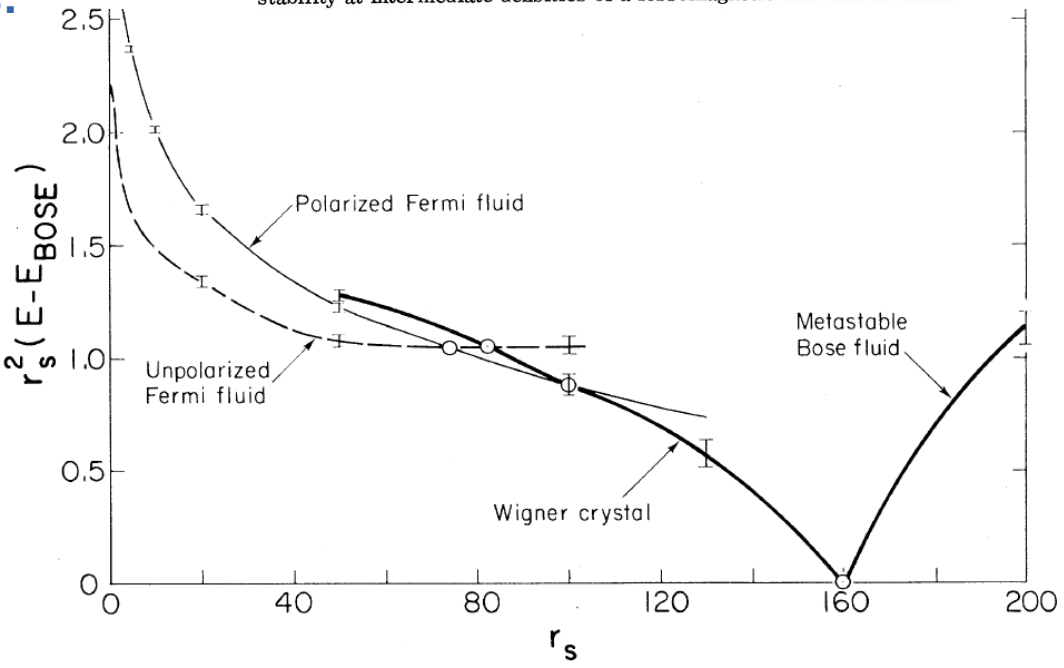

FIG. 2. The energy of the four phases studied relative to that of the lowest boson state times r_s^2 in rydbergs vs r_s in Bohr radii. Below $r_s = 160$ the Bose fluid is the most stable phase, while above, the Wigner crystal is most stable. The energies of the polarized and unpolarized Fermi fluid are seen to intersect at $r_s = 75$. The polarized (ferromagnetic) Fermi fluid is stable between $r_s = 75$ and $r_s = 100$, the Fermi Wigner crystal above $r_s = 100$, and the normal paramagnetic Fermi fluid below $r_s = 75$.

Methodological developments….:

Better ground state wave functions:

Slater-Jastrow

Ceperley, Chester, Kalos (1977)

$$\Psi_{SJ}(\mathbf{R}) = \det_{\mathbf{k}i} \phi_{\mathbf{k}}(\mathbf{r}_i) \exp\left[-U_2\right]$$

$$U_2 = \sum_{i<j} u_2(\mathbf{r}_i - \mathbf{r}_j)$$

Backflow - 3body

Schmidt,Pandharipande,.

$$\mathbf{q}_A(\mathbf{R}) = \mathbf{r}_A + \sum_i (\mathbf{r}_A - \mathbf{r}_i)\eta(\mathbf{r}_A - \mathbf{r}_i)$$

$$\Psi_{bf3}(\mathbf{R}) = \det_{\mathbf{k}i} \phi_{\mathbf{k}}(\mathbf{q}_i) \exp\left[-U_2 - U_3\right]$$

$$U_3 = \lambda \sum_i \left[\sum_{j\neq i} (\mathbf{r}_i - \mathbf{r}_j)\nu(\mathbf{r}_i - \mathbf{r}_j)\right]\left[\sum_{j\neq i} (\mathbf{r}_i - \mathbf{r}_j)\nu(\mathbf{r}_i - \mathbf{r}_j)\right]$$

- Higher many-body correlations: U_4,...
- Iterated backflow $q^{(n+1)}$ build by building functions from previous backflow coordinates $q^{(n)}$

→ Neural quantum states
- Graph neural networks
- Deep layer structures

See Shiwei Zhang, Yubo Yang, David Linteau, Conner Smith

Thermodynamic limit extrapolations: from finite (small) N to “real matter”

- Twisted boundary conditions (k-point sampling): eliminates/reduces shell effects
- Understanding of two-body correlations: finite-size corrections to reduce 2-body effects

Benchmark HEG N=14
IBF, WAP-net, FermiNet, MP-NQS, FCI...

M. Wilson, S. Moroni, M. H., N. Gao, F. Wudarski, T. Vegge, A. Bhowmik,Phys. Rev. B 107, 235139 (2023).

High density r_s<5

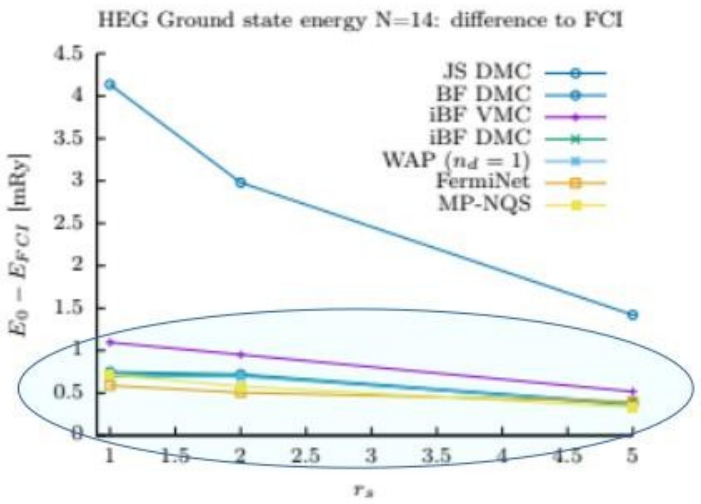

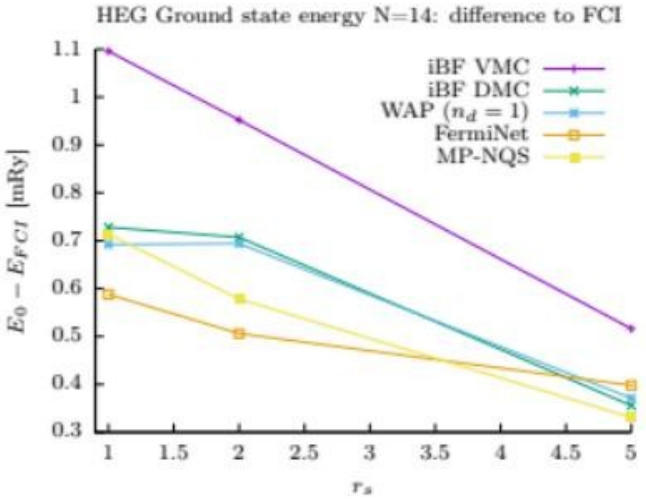

low density r_s>5

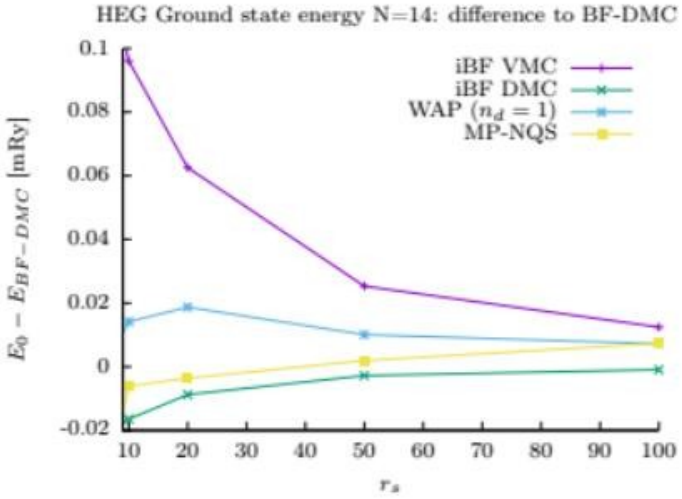

FCI:
K. Liao, T. Schraivogel, H. Luo, D. Kats, A. Alavi,
Phys. Rev. Research 3, 033072 (2021).

FermiNet:
G. Cassella, H. Sutterud, S. Azadi, N. D. Drummond,
D. Pfau, J. S. Spencer, W. M. C. Foulkes,
Phys. Rev. Lett. 130, 036401 (2023).

MP-NQS:
G. Pescia, J. Nys, J. Kim, A. Lovato, G. Carleo,
arXiv 2305.07240 (2023).

Phase diagram of the homogeneous electron gas:

Itinerant magnetism in 3D electron gas?

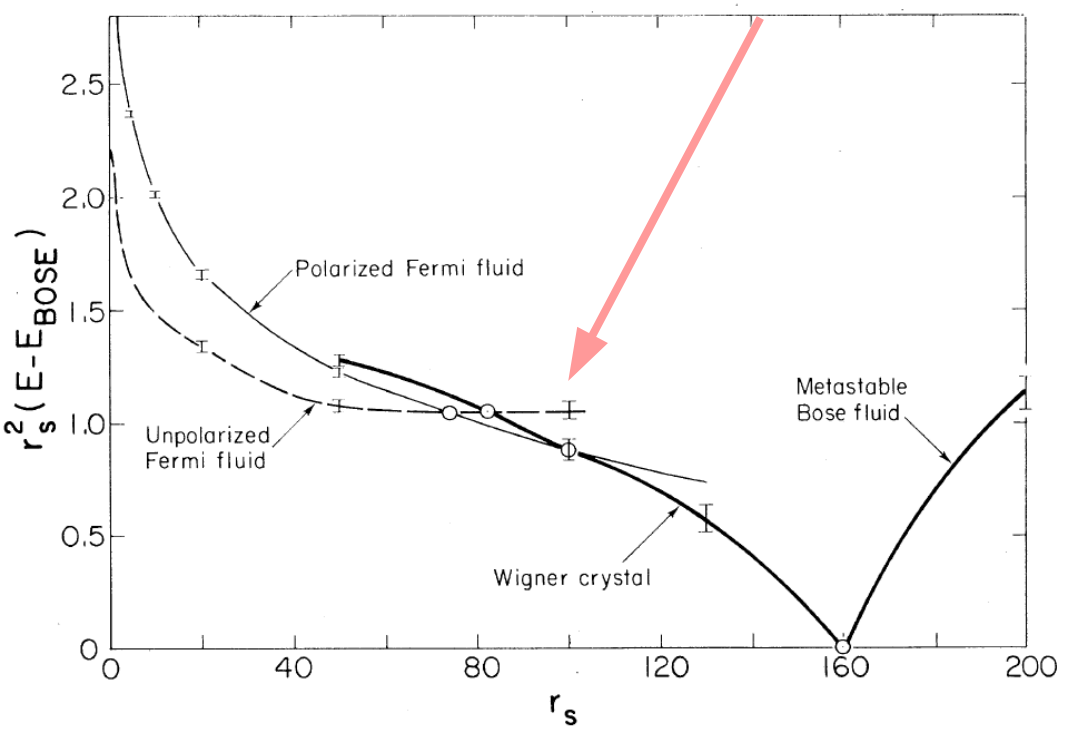

FIG. 2. The energy of the four phases studied relative to that of the lowest boson state times r_s^2 in rydbergs vs r_s in Bohr radii. Below $r_s = 160$ the Bose fluid is the most stable phase, while above, the Wigner crystal is most stable. The energies of the polarized and unpolarized Fermi fluid are seen to intersect at $r_s = 75$. The polarized (ferromagnetic) Fermi fluid is stable between $r_s = 75$ and $r_s = 100$, the Fermi Wigner crystal above $r_s = 100$, and the normal paramagnetic Fermi fluid below $r_s = 75$.

Itinerant ferromagnetism:

- F. Bloch (1929): F. Bloch, Zeitschrift f. Physik 57, 545 (1929).

  same electrons can lead to electronic conduction and ferromagnetism

  based on homogeneous electron gas model
  using Hartree-Fock approximation

- E. Wigner (1934): E. P. Wigner, Phys. Rev. 46, 1002 (1934)

  importance of correlations (beyond Hartree Fock)

  possibility of crystalline order at low densities (Wigner crystal)

  ”magnitude of correlation energy important for questions of para- and ferromegnetism”

- E. Stoner (1938): E.C. Stoner, Proc. R. Soc. Lond. A 165, 372 (1938)

  mimic correlations by phenomenological interaction term between
  spin-up and spin-down densities
  => continuous transition between zero and full magnetisation
  (Stoner transition)
  ”Stoner criterium”: ratio of repulsive energy to Fermi energy

Results from 2002 indicate Stoner transition!

Continuous
polarization transition at T=0

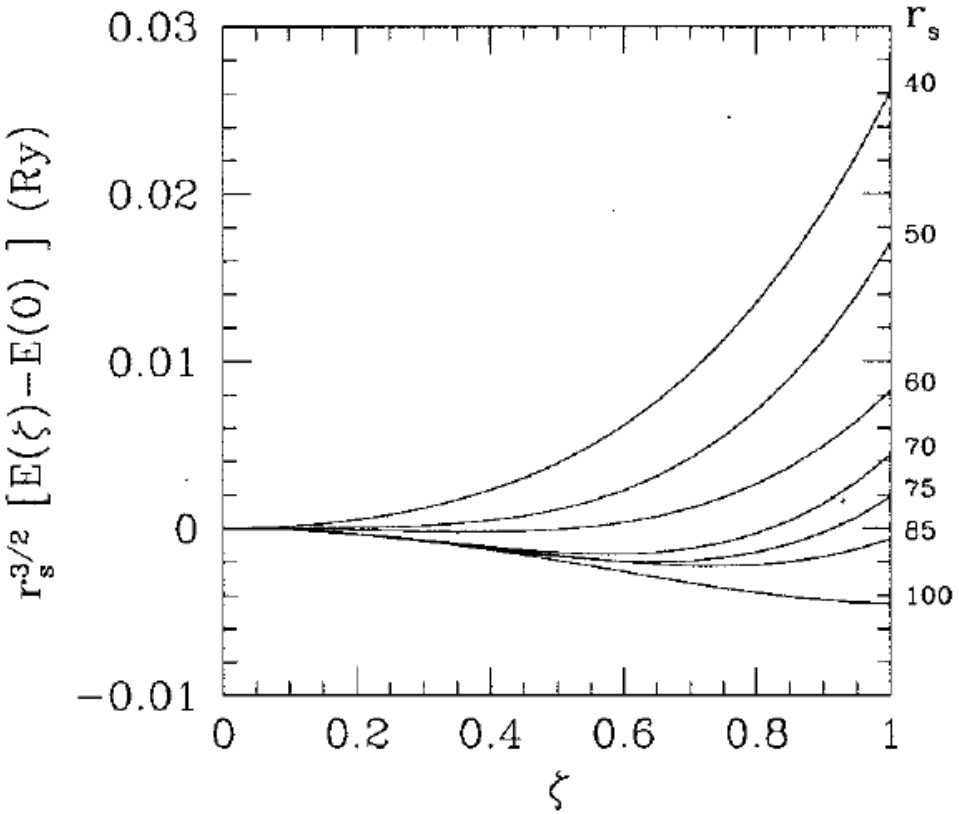

F. H. Zong, C. Lin, and D. M. Ceperley,
Phys. Rev. E 66, 036703 (2002)

Phase diagram T≥0

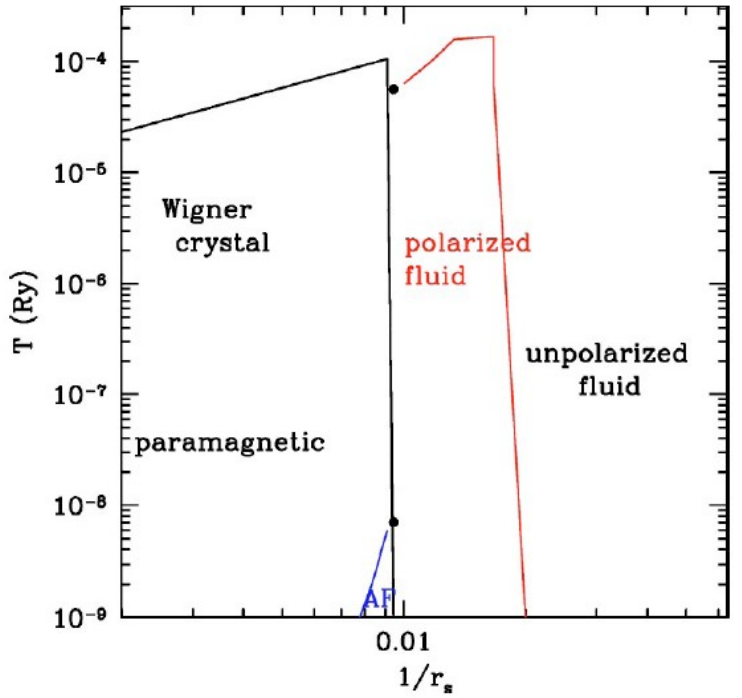

FIG. 1. (Color online) Phase diagram of the 3D electron gas showing the region of stability of the crystal (Ref. 7), the polarization transition from QMC calculations (Ref. 5), and the antiferromagnetic transition (this work).

B. Bernu, L. Candido, and D. M. Ceperley,
Phys. Rev. B 70, 094413 (2004)

Application of iterated backflow renormalization:

Itinerant magnetism in 3D electron gas?
Many-body correlations vs Stoner (polarization) transition

M.H. and S. Moroni, Phys. Rev. Lett. 124, 206404 (2020)

Many-body correlations in the low
Density region can be accurately
Extrapolated by iterative backflow

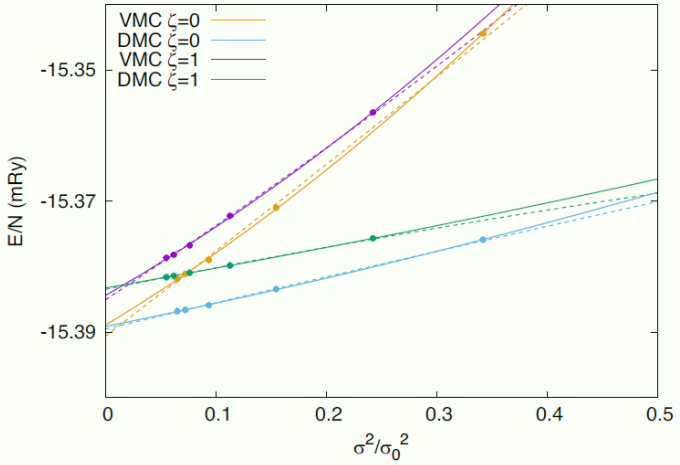

FIG. 1. Extrapolation of the energy to zero variance for $r_s = 100$ at polarizations $\zeta = 0$ and 1. The data are calculated with VMC and DMC using SJ, BF0, …, BF4 wave functions in order of decreasing energy. The reference value σ_0^2 is the variance of the local energy at $\zeta = 0$ with the SJ wave function. The curves are quadratic fits; for each set of data points (VMC and DMC for $\zeta = 0$ and 1) there are two curves, one of which (solid line) excludes the SJ energy from the fit.

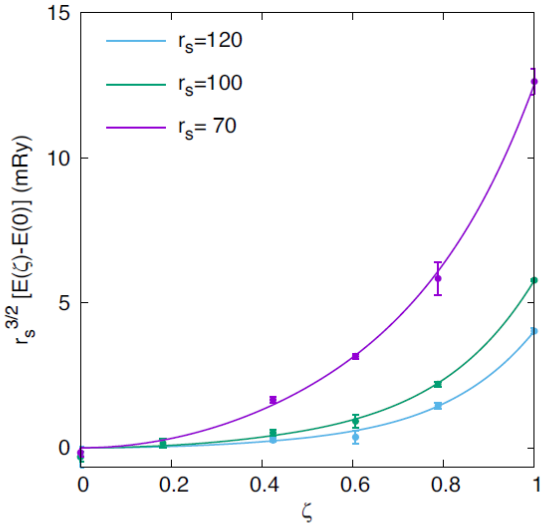

FIG. 3. The polarization energy $E(\zeta) - E(0)$ obtained from zero-variance extrapolations of the DMC energies without the SJ result. The lines are polynomial fits with terms of order 0, 2, and 6. Alternative functional forms and ensuing confidence levels for

Wigner crystalization
sets in before
Polarization transition

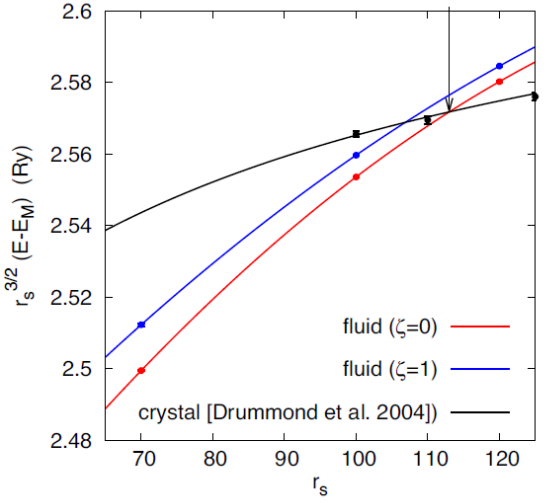

Does a Stoner transition occur in nature?

- Electronic systems:
  itinerant ferromagnetism: correlations + band structure

- different isotropic systems with spin-independent ?
  (ultracold atoms/ molecules)

  - Change scattering length $a_s \to \infty$?
    => difficulties/controversals due to 2-body bound state leading to instability!

  - Dipolar interactions (heteronuclear molecules, Rydberg atoms)?
    => no polarization transition in 2D before freezing

    T. Comparin, R. Bombin, M. H., F. Mazzanti, J. Boronat, and S. Giorgini, Phys. Rev. A 99, 043609 (2019)

- Liquid helium ? No
  experiment / higher order backflow calculations...

Conjecture:
For an isotropic normal Fermi liquid with
spin-independent isotropic interactions
the ground state remains unpolarized up to freezing.

Beyond ground state energies:

- Quantum Monte Carlo calculations are based on variational principle
  - Energy is true upper bound, but other (ground) state properties are accessible: pair correlation functions, static structure factor give structural information

    Momentum distribution gives complementary information:
    Extended or localized electronic states, Fermi liquid behavior?

  - Extensions to excited state properties:
    effective mass, gaps?

- (New) difficulties for computing spectral properties:
  - QMC extensions for excited states to guarantee orthogonality

  - Extended systems/thermodynamic limit: continuous spectrum:
    important finite size effects may be expected,
    transition from discrete to continuous spectra might not be straightforward

Momentum distribution of the homogeneous electron gas in 3D (3DEG): G_0W_0, QMC, experiment...

S. Huotari, J. A. Soininen, T. Pylkkänen, A. Titov, A. Issolah, K. Hämäläinen, J. McMinis, J. Kim, K. Esler, D.M. Ceperley, M. H., and V. Olevano, Phys. Rev. Lett. 105, 086403 (2010).

valence electrons in Na ≈ 3DEG

- Na: very isotropic valence band
- spherical Fermi surface: anisotropies around k_F <≈0.2%

momentum distribution can be measured
via inelastic X-ray scattering
(Compton profile)

Compton profile from inelastic X-ray scattering

scattering cross section:

$$\frac{d^2\sigma}{d\Omega d\omega_2} = \left(\frac{d\sigma}{d\Omega}\right)_{Th} S(\mathbf{k},\omega)$$

dynamic structure factor

high energies (synchrotron): impulsive approximation

$$S(\mathbf{k},\omega) \simeq J_{\hat{\mathbf{k}}}\left(\omega/k - k/2\right)$$

Compton profile

$$J_{\mathbf{k}}(q) = \int d^3\mathbf{p}\, n(\mathbf{p})\delta(\mathbf{p}\cdot\hat{\mathbf{k}} - q)$$

spherical averaged Compton profile

$$J(q) = \int_{|q|}^{\infty} d^2\mathbf{p}\, n(\mathbf{p})$$

momentum distribution n(k) by differentiation

renormalization factor Z gives kink

Valence electron Compton profile of Na: experiment

subtract contribution of core electrons

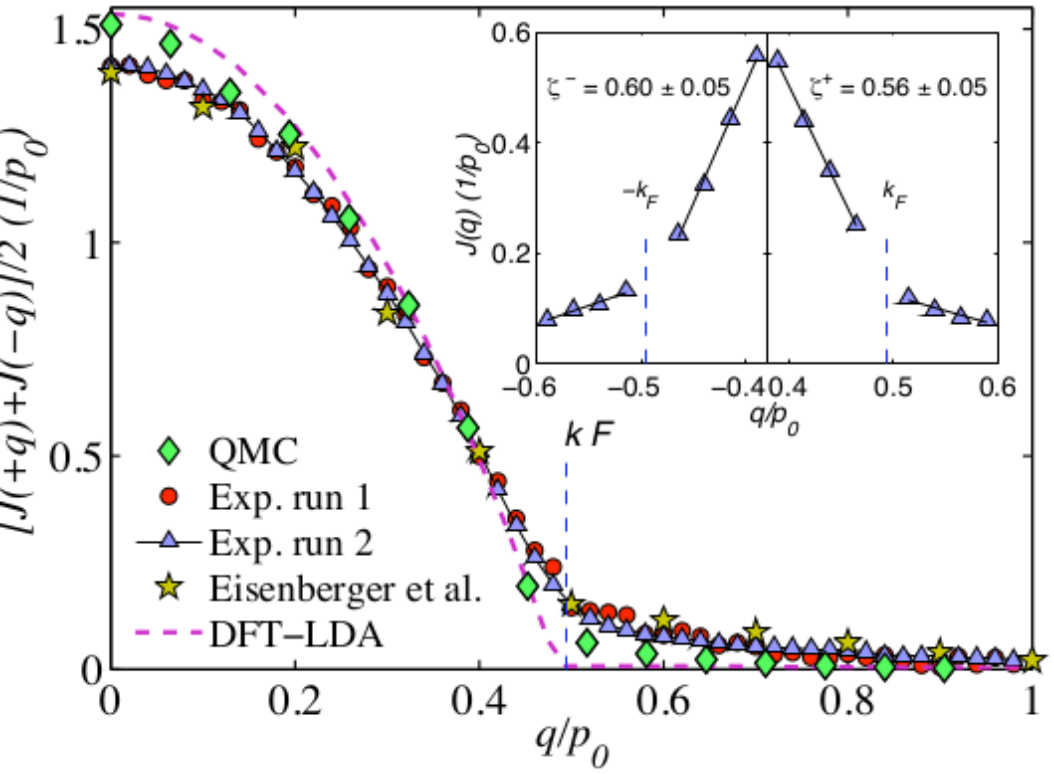

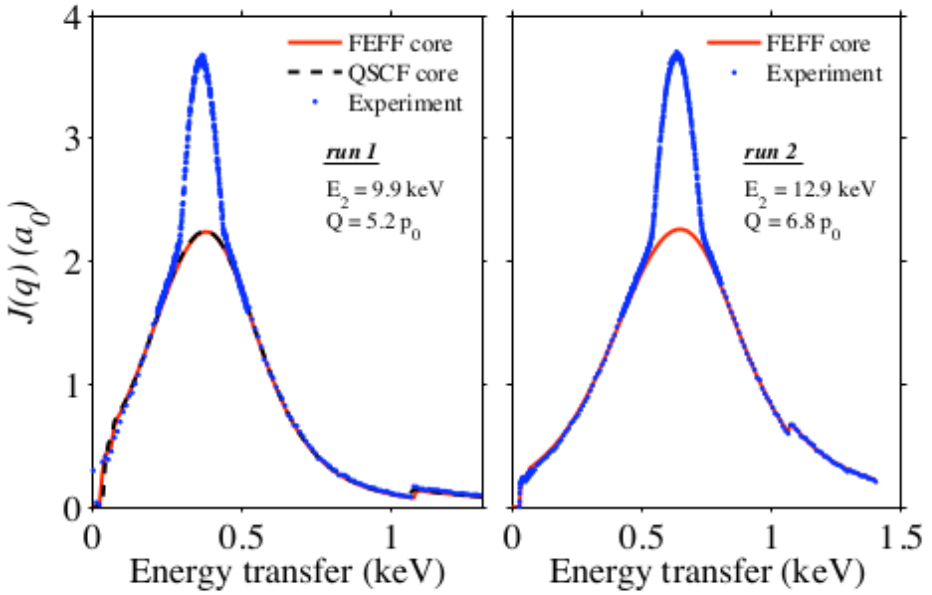

FIG. 2 (color online). The measured x-ray-scattering spectra from Na as a function of energy transfer, for both experimental runs. The experimental spectra consist of overlapping valence and core contributions. Theoretical core contributions are shown for both QSCF and FEFFQ treatments.

discontinuity in the slope at k_F: direct measurement of Z and k_F

momentum distribution of Na
renormalization factor Z of 3DEG at r_s=3.99

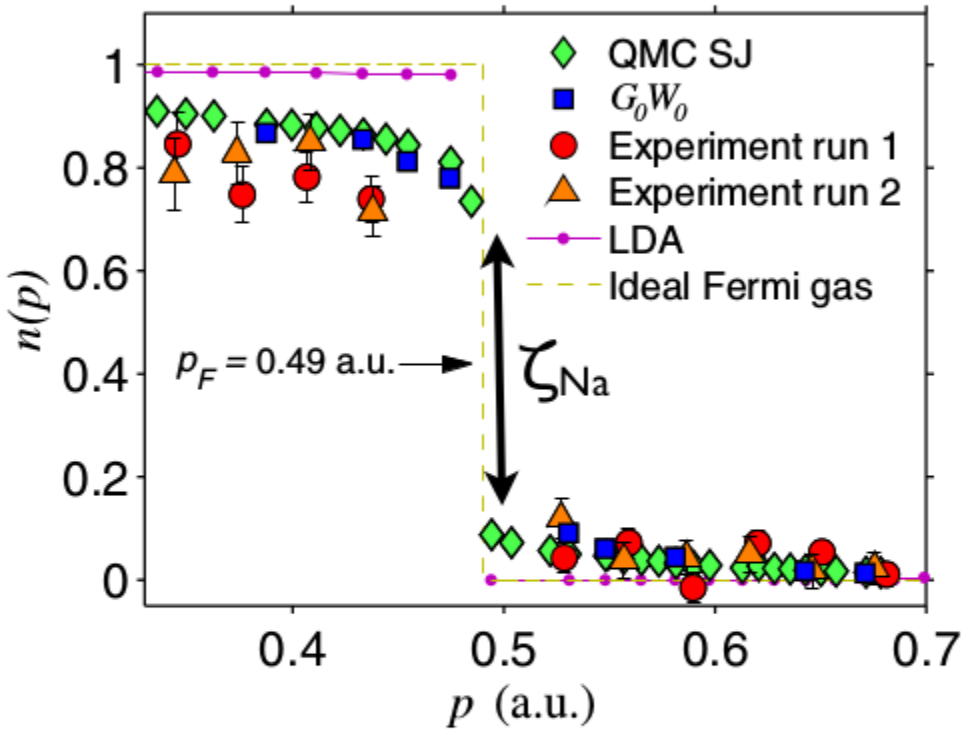

FIG. 1 (color online). The momentum distribution of Na determined by experiment, QMC SJ, G_0W_0, and LDA calculations. The ideal-Fermi gas step function is also shown.

valence electron density:
r_s=3.99

QMC and G_0W_0 indicate
that bandstructure and correlation effects
factorize at k_F

$$\zeta_{\mathrm{Na}} = |\tilde{\phi}^{\mathbf{G}=0}_{\nu=1,\mathbf{k}_F}|^2 Z_{\mathbf{k}_F}$$

LDA bandstructure wfn-coeff.

$Z_{Na} \cong Z_{3DEG}$

Technique	ζ^{Na}	$Z^{Na}_{k_F}$	$Z^{HEG}_{k_F}$
Experiment	0.57(7)	0.58(7)	
QMC SJ	0.68(2)	0.70(2)	0.69(1)
QMC BF			0.66(2)
G_0W_0	0.64(1)	0.65(1)	0.64 [2]
GW [6]			0.793
RPA (on shell)			0.45
expS_2 [4]			0.59
EPX [8]			0.61
Lam [5]			0.615
FHNC [7]			0.71

comparision with theories

Momentum distribution of solid and liquid Li (r_s=3.25): Experiment vs QMC (full electron)

Yang, Hiraoka, Matsuda, M. H., Ceperley,
Phys. Rev. B 101, 165125 (2020);
Hiraoka, **Yang**, Hagiya, Niozu, Matsuda, Huotari, M. H., Ceperley,
Phys. Rev. B 101, 165124 (2020).

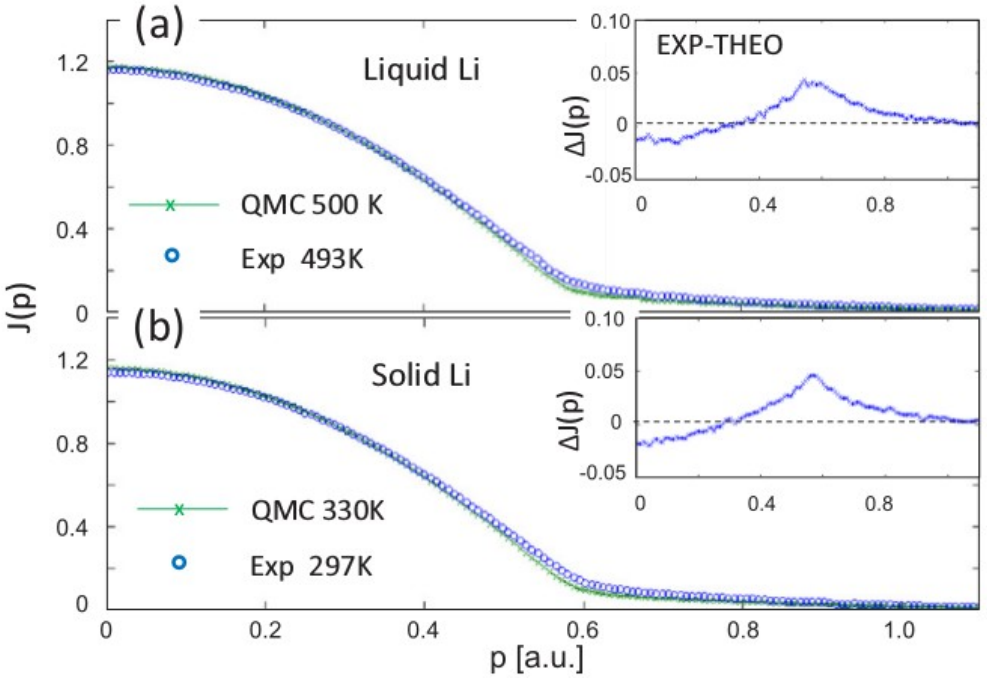

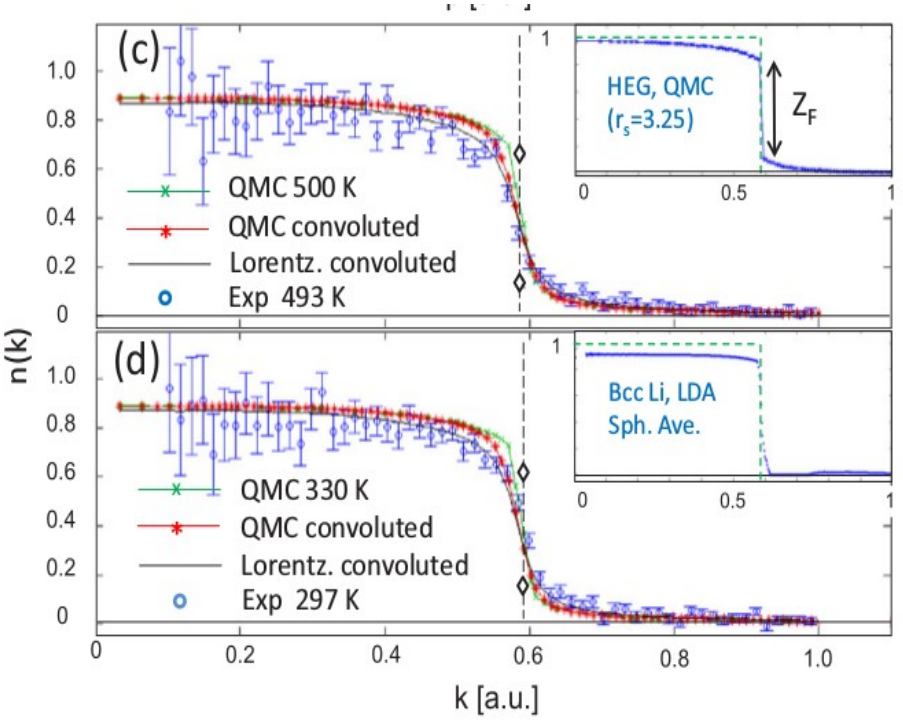

FIG. 2. Valance CPs of liquid (a) and solid Li (b), compared with theory convoluted by the broadening function. The insets show the difference between the experimental and theoretical CPs. EMDs in liquid (c) and solid Li (d), compared to theory with or without the convolutions. The insets show EMD for HEG and the spherically averaged EMD from band theory (LDA). The ◊'s in (c) and (d) show the $n(k_F)$ obtained by RPA fits near k_F.

Use of Pseudo-potentials to eliminate core electrons gives systematic (small) deviations: all electron calculations needed!

Landau-Fermi Liquid (I)

Ideal Fermions:

occupation number:
Fermi-Dirac distribution

$$n_{k\sigma} = \frac{1}{e^{(\hbar^2 k^2/2m - \mu)/T} + 1}$$

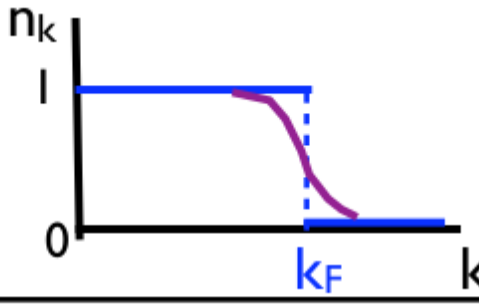

- Observation:

  Low Temperature Properties of a Fermi liquid (^{3}He)

  ≈ ideal Fermi gas with renormalized parameters

- Interacting Fermions postulating quasi-particles:

single particle dispersion with effective mass m*

$$\varepsilon^0_{k\sigma} = \frac{\hbar^2 k_F}{m^*}\left(|\mathbf{k}| - k_F\right)$$

$$E(\delta n_{k\sigma}) = E_0 + \sum_{k,\sigma} \varepsilon^0_{k\sigma}\delta n_{k\sigma} + \frac{1}{2V}\sum_{k\sigma k'\sigma'} f_{k\sigma,k'\sigma'}\delta n_{k\sigma}\delta n_{k'\sigma'} + \ldots$$

quasi-particle interactions, necessary for consistency!

Landau-Fermi Liquid (II)

- quasi-particle occupation δn_k :
  - adiabatically connected to ideal gas occupation
  - not directly observable
- parameters [m*, f(k,k)] at k_F determined by few measurments
  (specific heat C, compressibility, magnetic susceptibility,...)

  $\Rightarrow$ predicitions

  for transport properties, ...

→ Limits of applicability?

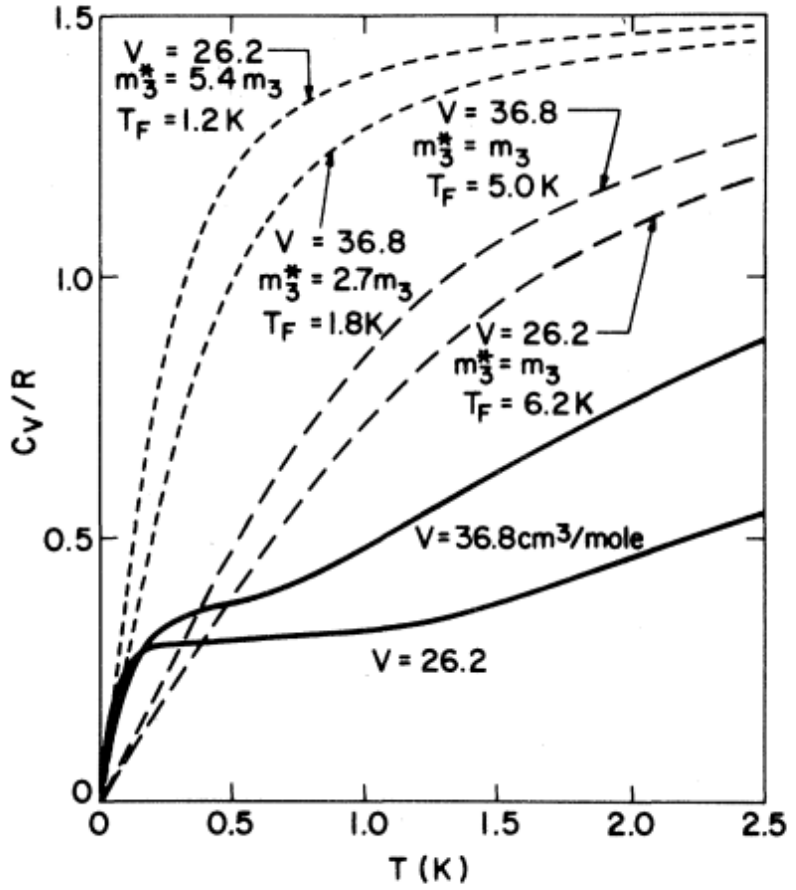

specific heat of liquid ^3He

D. Greywall PRB 27, 2747 (1983)

QMC attemps to match excitation spectra to Landau functional

$$\delta E = \sum_{p\sigma} (\varepsilon_p + \mu)\delta n_{p\sigma} + \frac{1}{2V} \sum_{p\sigma, p'\sigma'} f(p\sigma, p'\sigma')\delta n_{p\sigma}\delta n_{p'\sigma'}$$

- Controversy of m*:
  VdiagMC,K. Haule and K. Chen,
  Scientific Reports 12, 2294 (2022)
  vs QMC study by
  Azadi, Drummond, Foulkes
  PRL 127, 086401 (2021)

- Problems:

  - No explicit (operational) definition of quasi-particle excitation
  - Validity away from the Fermi surface?
  - Non degenerate ideal gas excitations only for finite N around Fermi surface
  - Discrete (finite N) vs continuous (infinite N) energy spectrum of excitations:
    m* characterizes the continuous spectrum!

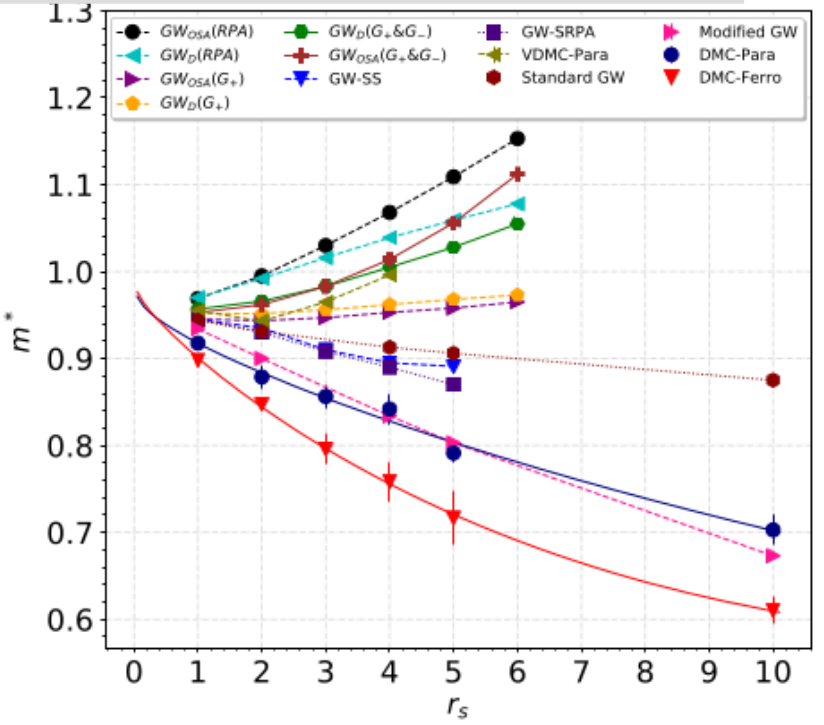

FIG. 4. Quasiparticle effective masses m^* of paramagnetic (Para) and ferromagnetic (Ferro) 3D HEGs at the infinite-system-size limit as functions of density parameter r_s. Padé functions were fitted to the DMC quasiparticle energy bands to determine the effective mass. The many-body GW_x and variational diagrammatic Monte Carlo (VDMC) results are from Refs. [52] and [53], respectively. The *GW* SS and *GW* SRPA results are from Refs. [54] and [55], respectively. The "standard *GW*" data and "modified *GW*" data are taken from Ref. [56]. All the *GW* results are for paramagnetic 3D HEGs.

Fermi Liquid: Microscopic Description (I)

Single particle Green's function: $G_R(k,t) \equiv -i \left\langle e^{iHt} a_k e^{-iHt} a_k^\dagger \right\rangle \theta(t)$

$$= \int \frac{d\omega}{2\pi} G_R(k,\omega) e^{-i\omega t}$$

$$G_R(k,\omega) = \sum_n \frac{\left| \left\langle n | a_k^\dagger | 0 \right\rangle \right|^2}{\omega - (E_n^{N+1} - E_0^N - \mu) + i\eta}$$

excitation energies ➠ peaks in spectral function

$$A(k,\omega) = -\frac{1}{\pi} \mathrm{Im} G_R(k,\omega)$$ (measured in ARPES)

ideal gas

$$A_0(k,\omega) = \delta(\omega - \mu - k^2/2m)$$

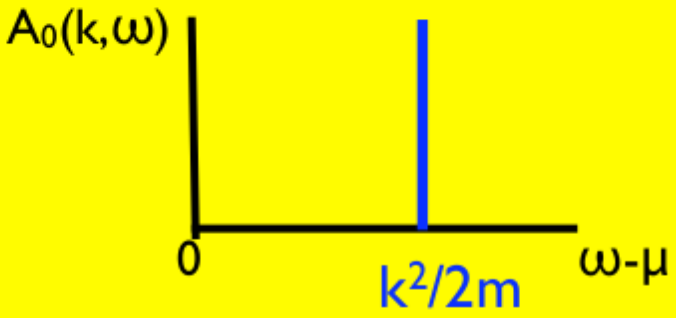

interacting system

$$A_0(k,\omega) = \frac{Z_k}{2\pi} \frac{\tau_k^{-1}}{(\omega - \mu - \varepsilon_k)^2 + (2\tau_k)^{-2}} + A_{\mathrm{inc}}$$

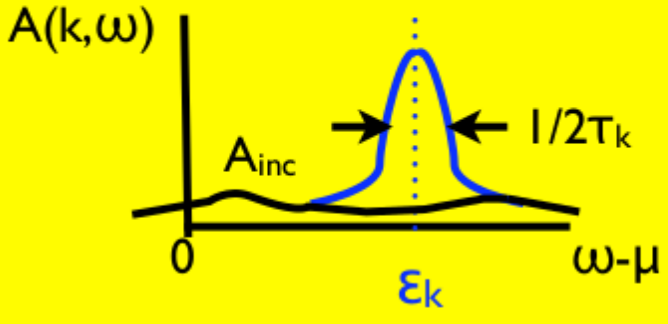

Fermi Liquid: Microscopic Description (II)

Self-energy Σ(k,ω): $G^{-1}(k,\omega) = \omega - \mu - k^2/2m - \Sigma(k,\omega)$

form of G around quasi-particle peak $G^{-1}(k, \omega - \mu \approx \varepsilon_k) = Z_k^{-1}(\omega - \mu - \varepsilon_k + i\tau_k/2)$

quasi-particle energy: $\varepsilon_k = k^2/2m + \mathrm{Re}\,\Sigma(k, \mu + \varepsilon_k)$

inverse quasi-particle weight: $Z_k^{-1} = 1 - \partial \mathrm{Re}\,\Sigma(k, \mu + \varepsilon_k)/\partial\omega$

inverse lifetime: $\tau_k^{-1} = -2Z_k\,\mathrm{Im}\,\Sigma(k, \mu + \varepsilon_k)$

Definition of Fermi liquid: $\tau_k^{-1} \to 0 \quad \text{for} \quad k \to k_F$

Delta function excitation at the Fermi surface $A(k \to k_F, \omega \approx \mu) = Z_k \delta(\omega - \mu - k^2/2m^*)$

$m/m^* = Z_{k_F}\,(1 + m/k_F\,\partial\Sigma(k_F, \mu)/\partial k)$

with effective mass m* from expansion around $\omega - \mu = \varepsilon_k \equiv k^2/2m*$

$\Sigma(k, \mu + \varepsilon_k) = \Sigma(k_F, \mu) + (k - k_F)\partial\Sigma(k_F, \mu)/\partial k + \varepsilon_k \partial\Sigma(k_F, \mu)/\partial\omega + \ldots$

Fermi Liquid: Momentum Distribution n_k

Sharp jump of n_k at k_F is consequence of δ-function excitation at k_F

$$n_k \equiv \langle a_k^\dagger a_k \rangle = \int_{-\infty}^{\mu} d\omega A(k,\omega)$$

$k<k_F$: quasi-particle peak of A below μ

$p>k_F$: quasi-particle peak of A above μ

$$n_k - n_p \simeq Z_k + \int_{-\infty}^{\mu} d\omega \left[A_{inc}(k,\omega) - A_{inc}(p,\omega)\right]$$

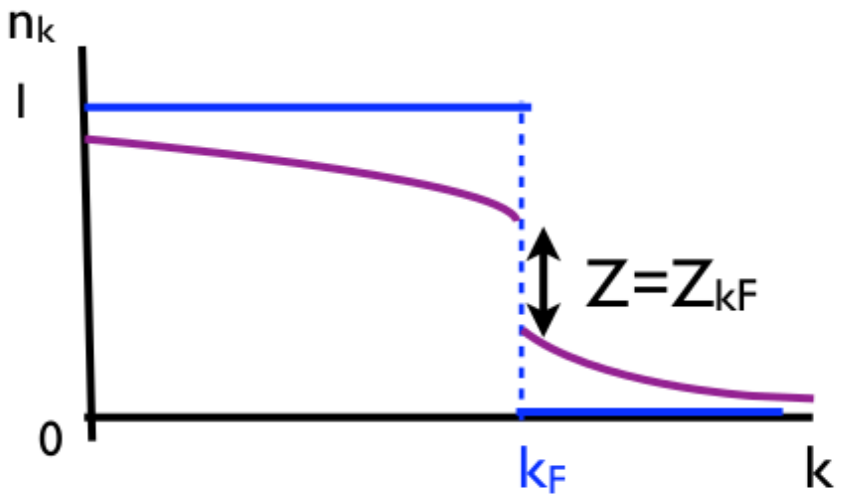

Microscopic Definition of m*

Def. from single particle Green's function

$$\frac{m}{m^*} = \frac{1 + \frac{m}{k_F}\frac{\partial \Sigma(k_F,\mu)}{\partial k}}{1 - \frac{\partial \Sigma(k_F,\mu)}{\partial \omega}}$$

Fermi liquids have jump Z in momentum distribution:

$$Z = \frac{1}{1 - \frac{\partial \Sigma(k_F,\mu)}{\partial \omega}}$$

✘ we calculate Z within QMC

❑ how to calculate k-derivative of self-energy? $\frac{\partial \Sigma(k_F,\mu)}{\partial k}$

➥note that Σ(k,μ) is a static quantity

and G(k,μ) is a static response function!

QMC calculation of the static self-energy (I)

QMC can calculate static response function remaining variational

VOLUME 69, NUMBER 13 PHYSICAL REVIEW LETTERS 28 SEPTEMBER 1992

Static Response from Quantum Monte Carlo Calculations

Saverio Moroni,[1],[a] David M. Ceperley,[1] and Gaetano Senatore[2]
[1] *National Center for Supercomputing Applications and Department of Physics, University of Illinois at Urbana-Champaign, Urbana, Illinois 61801*
[2] *Dipartimento di Fisica Teorica, Università di Trieste, Strada Costiera 11, I-34014 Trieste, Italy*
(Received 18 June 1992)

$$v_{\mathrm{ext}}(\mathbf{r}) = 2v_{\mathbf{q}} \cos(\mathbf{q}\cdot\mathbf{r}),$$

$$E_v = E_0 + \frac{\chi(q)}{n_0} v_{\mathbf{q}}^2 + C_4 v_{\mathbf{q}}^4 + \cdots.$$

adapt for single particle excitation:

add external potential ξ a_k^+ to Hamiltonian $H(\xi_k) = H - \mu N + \xi_k a_k^\dagger + \xi_k^* a_k$

and minimize energy using N/N+1 wave function $E(\xi_k) - E_0 = G(k,\mu)\,\xi_k^2$

$\Rightarrow$ static self-energy $\Sigma(k,\mu) = \mu - G^{-1}(k,\mu) - k^2/2m$

QMC calculation of the static self-energy (II)

$$H(\xi_k) = H - \mu N + \xi_k a_k^\dagger + \xi_k^* a_k$$

$$E_0(\xi_k) \leq \frac{\langle \Psi_k | H(\xi_k) | \Psi_k \rangle}{\langle \Psi_k | \Psi_k \rangle}$$

ansatz for wave function: $\Psi_k(\mathbf{R}) = \psi_0^N(\mathbf{R}_N) + \alpha_k \psi_k^{N+1}(\mathbf{R}_{N+1})$

$$E_0(\xi_k) = E_0 - \frac{z_k}{E_k^{N+1} - E_0^N - \mu} \xi_k^2, \quad \text{for } \xi_k \to 0$$

$$z_k = \frac{|\langle \psi^{N+1} | a_k^\dagger | \psi_0^N \rangle|^2}{\langle \psi_0^N | \psi_0^N \rangle \langle \psi_k^{N+1} | \psi_k^{N+1} \rangle} \qquad E_k^{N+1} = \frac{\langle \psi_k^{N+1} | H \psi_k^{N+1} \rangle}{\langle \psi_k^{N+1} | \psi_k^{N+1} \rangle}$$

chose wave function such that:

a) minimize energy difference $E_k^{N+1} - E_0^N - \mu$ $\quad \phi_k^{N+1}(\mathbf{R}_{N+1}) = \det_{ik} \varphi_k(\mathbf{q}_i) e^{-U_{N+1}}$

b) maximize overlap z_k $\quad a_k^\dagger \psi_0^N(\mathbf{R}_N)$

Static self-energy

M.H., F. Calcavecchia, D.M. Ceperley, V. Olevano, cond-mat 2305.02274 (2023)

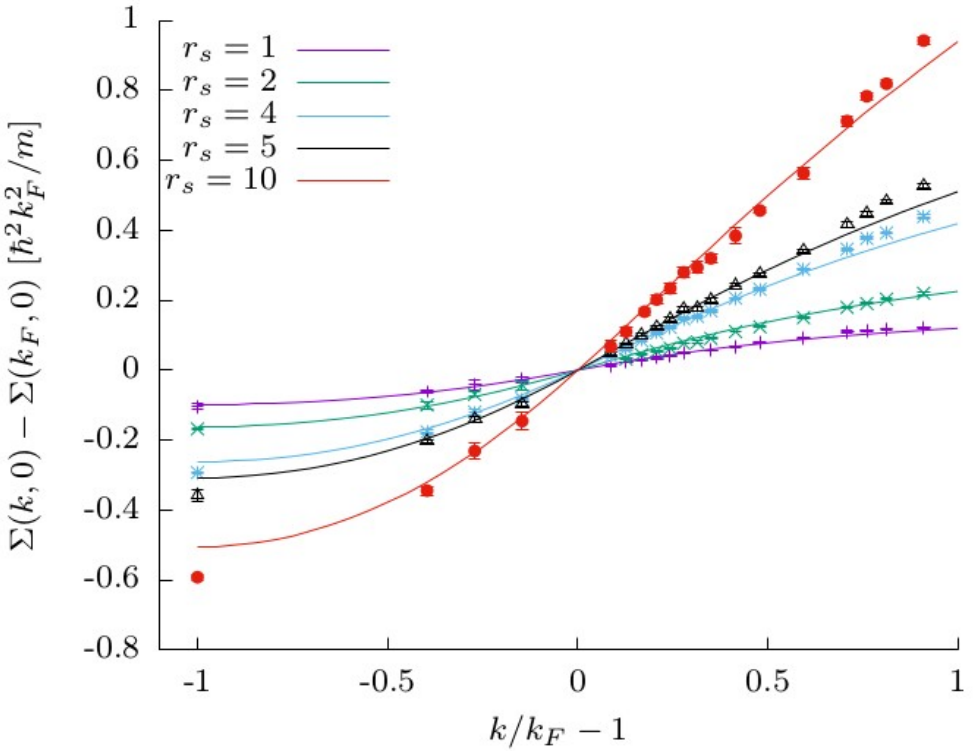

FIG. 1: Static self-energy for various densities (r_s) using backflow (BF) trial wave functions and GC-TABC simulations for $N = 38$ electrons. They include size corrections. The color lines are from G_0W_0 calculations.

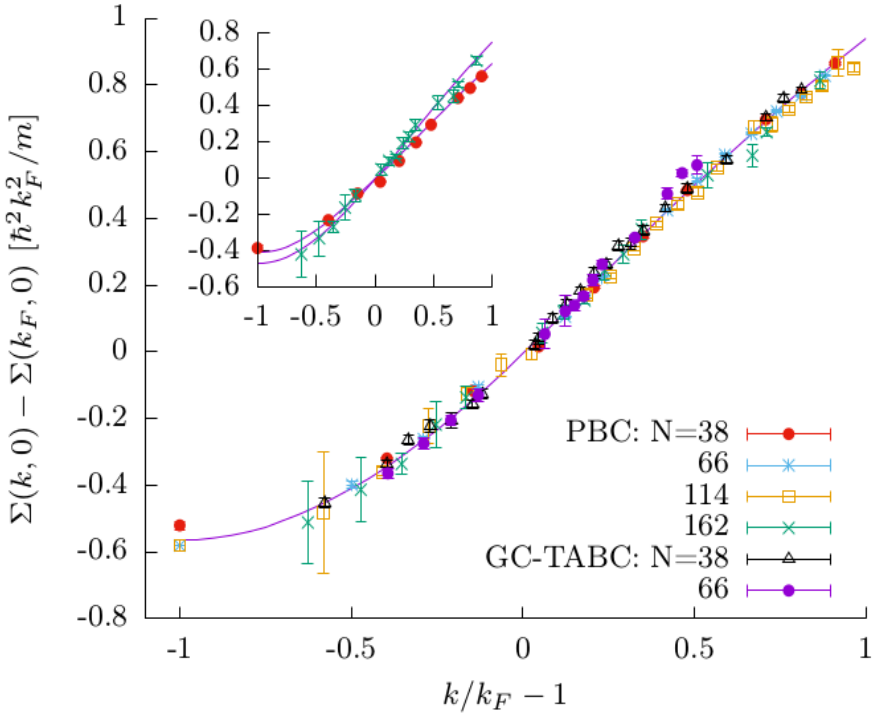

FIG. 2: Static self-energy for $r_s = 10$ using SJ-VMC trial wave functions for simulations with periodic boundary conditions (PBC) and GC-TABC for various sizes ranging from $N = 38$ to $N = 162$, size corrected according to Eq. (17), the line is a fit to the data. The inset shows the uncorrected values for $N = 38$ and $N = 162$ (PBC), the lines indicate the size corrections of the fit based on Eq. 17).

Size corrections (analytic):

M. H., B. Bernu, D. Ceperley, J. Phys.: Conf. Ser. 321 012020 (2011), cond-mat/1105.2964.

4.2. Renormalization factor and effective mass

For the calculation of the renormalization factor and the effective mass, we need the derivatives of the self energy at the Fermi surface. Within the RPA, we have

$$\frac{\partial\Sigma(k_F,\varepsilon_F)}{\partial\omega} = -\frac{1}{V}\sum_{\mathbf{q}\neq 0}\int_{-\infty}^{\infty}\frac{d\nu}{(2\pi)}\left[\frac{1}{\epsilon(q,i\nu)}-\frac{1}{\epsilon(q,0)}\right]\frac{v_q}{[i\nu+\varepsilon_F-\varepsilon_{k_F+\mathbf{q}}]^2} \qquad (19)$$

$q\to 0$

$$\frac{m}{k_F}\frac{\partial\Sigma(k_F,\varepsilon_F)}{\partial k} = \frac{1}{V}\sum_{\mathbf{q}\neq 0}\int_{-\infty}^{\infty}\frac{d\nu}{(2\pi)}\frac{1}{\epsilon(q,i\nu)}\frac{v_q}{[i\nu+\varepsilon_F-\varepsilon_{k_F+\mathbf{q}}]^2}\left[1+\frac{\mathbf{k}_F\cdot\mathbf{q}}{k_F^2}\right] \qquad (20)$$

➡ Leading order size corrections from Coulomb singularity (q⟶0)

Exact (beyond RPA) leading order finite size corrections (based on Ward identities):

$$\delta\Sigma(k,0) \simeq -\int_{-\pi/L}^{\pi/L}\frac{d^3q}{(2\pi)^3}\int_{-\infty}^{\infty}\frac{d\nu}{(2\pi)}\frac{v_q}{\epsilon(q,i\nu)}\frac{1}{i\nu+\mu-\varepsilon^0_{k+q}}$$

Z + static self-energy = m*

M.H., F. Calcavecchia, D.M. Ceperley, V. Olevano, PRL 131, 186501 (2023)

r_s	method	Z	$mk_F^{-1}\partial_k\Sigma$	m^*/m
1	BF-VMC	0.86(1) [13]	$0.17^{0.18}_{0.15}(1)$	$1.00^{1.01}_{0.99}(1)$
	SJ-VMC	0.894(9) [13]	$0.17^{0.18}_{0.15}(1)$	$0.96^{0.97}_{0.95}(1)$
	G_0W_0 (RPA)	0.859 [31]	0.200	0.970 [10]
	VDiagMC [12]	0.8725(2)	0.200(1)	0.955(1)
2	BF-VMC	0.78(1)	$0.309^{0.361}_{0.280}(6)$	$0.98^{1.00}_{0.94}(1)$
	SJ-VMC	0.82(1)	$0.30^{0.31}_{0.28}(2)$	$0.94^{0.95}_{0.93}(2)$
	G_0W_0 (RPA)	0.768 [31]	0.313	0.992 [10]
	VDiagMC [12]	0.7984(2)	0.328(4)	0.943(3)
4	BF-VMC	0.65(1)	$0.538^{0.549}_{0.530}(7)$	$1.00^{1.01}_{0.99}(2)$
	SJ-VMC	0.69(1)	$0.55_{0.45}(2)$	$0.94^{1.00}(2)$
	G_0W_0 (RPA)	0.646 [31]	0.490	1.039 [10]
	VDiagMC [12]	0.6571(2)	0.528(5)	0.996(3)
5	BF-VMC	0.59(1)	$0.56^{0.65}(1)$	$1.09_{1.03}(3)$
	SJ-VMC	0.61(1)	$0.610^{0.624}_{0.596}(9)$	$1.02^{1.03}_{1.01}(2)$
	G_0W_0 (RPA)	0.602 [31]	0.569	1.059 [10]
10	BF-VMC	0.41(1)	$0.90^{0.98}_{0.88}(2)$	$1.28^{1.30}_{1.23}(3)$
	SJ-VMC	0.45(1)	$0.97^{1.03}_{0.91}(3)$	$1.13^{1.16}_{1.09}(3)$
	G_0W_0 (RPA)	0.45 [31]	0.98	1.13

TABLE I: Our QMC results with backflow (BF) and Slater-Jastrow (SJ) trial functions as compared to those of G_0W_0 (RPA) and variational diagrammatic Monte Carlo (VDiagMC) [12, 32, 33]. Upper and low indices indicate systematic errors assuming different fitting functions/ranges to determine $\partial_k\Sigma(k_F, 0)$.

From ground states to excitations…..

High pressure hydrogen: Insulator-metal transition

- Characterize insulator: spectral (optical) properties, gaps,…
- CEIMC: includes nuclear quantum motion

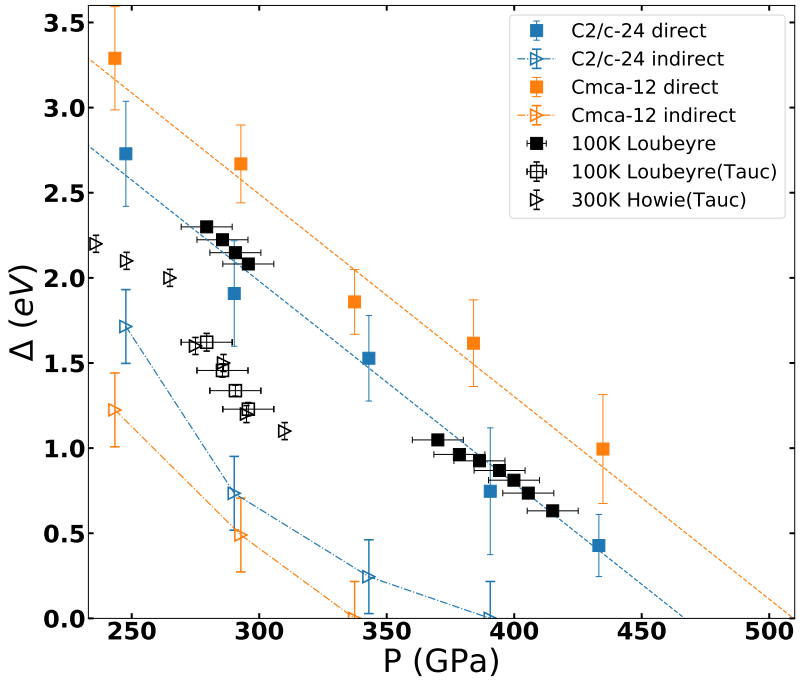

V. Gorelov, M. Holzmann, D. Ceperley, C. Pierleoni, PRL 124, 116401 (2020)

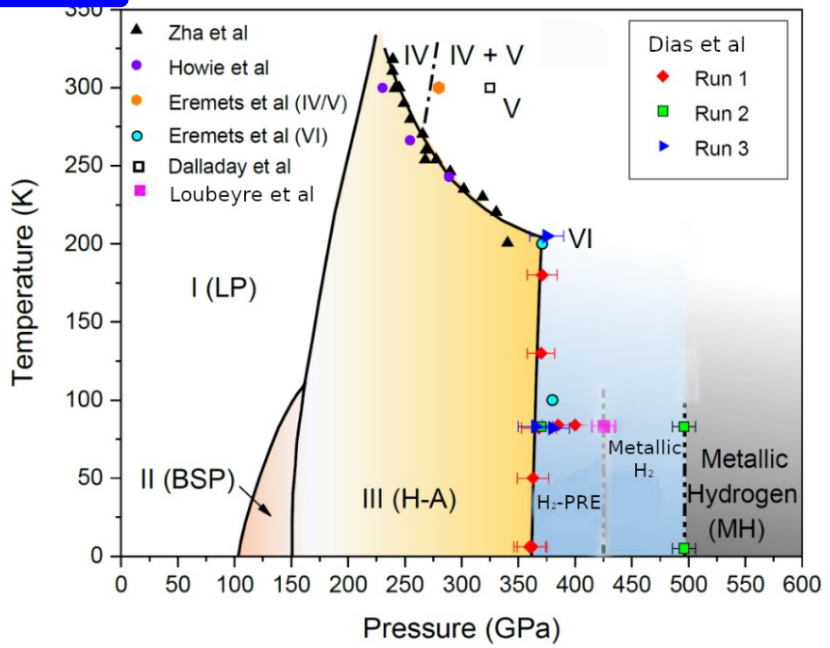

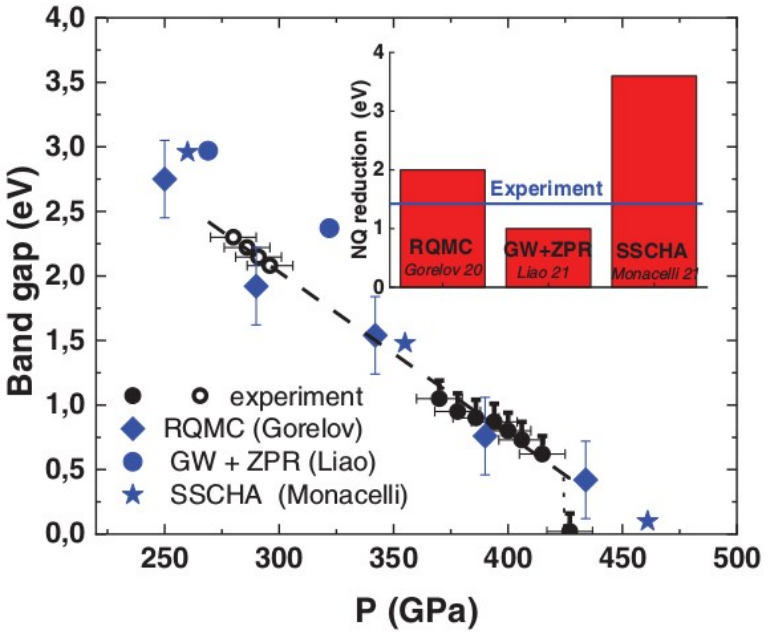

P. Loubeyre, F. Occelli , P. Dumas, PRL 129, 035501 (2022)

Electronic momentum distribution and fundamental gap at the LLPT

V. Gorelov, D. Ceperley, M.H., C. Pierleoni, PRB 195133 (2020)

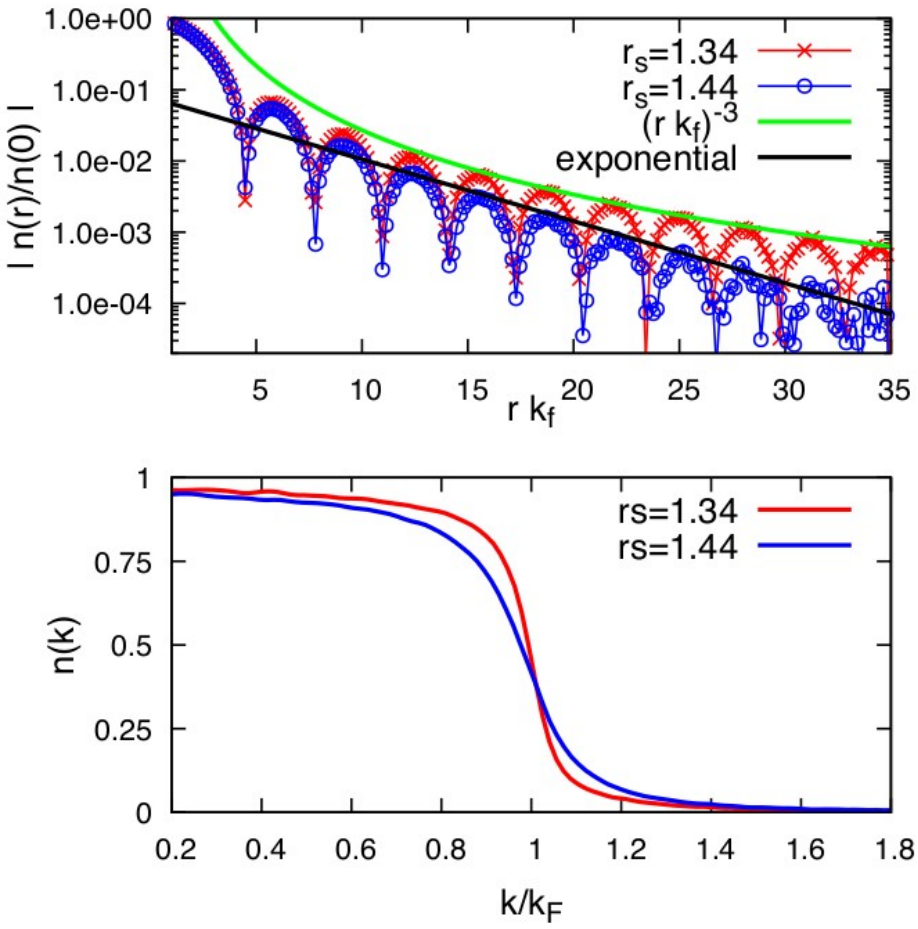

FIG. 30. Electronic momentum distribution of hydrogen at two densities across the LLPT at $T = 1200\,\mathrm{K}$, computed using a Slater-Jastrow backflow trial wavefunction with configurations from CEIMC. In the molecular phase (blue) the single-electron density matrix, $n(r)$, decreases exponentially with r, while in the dissociated phase (red) it decreases as r^{-3} because the electrons are delocalized.

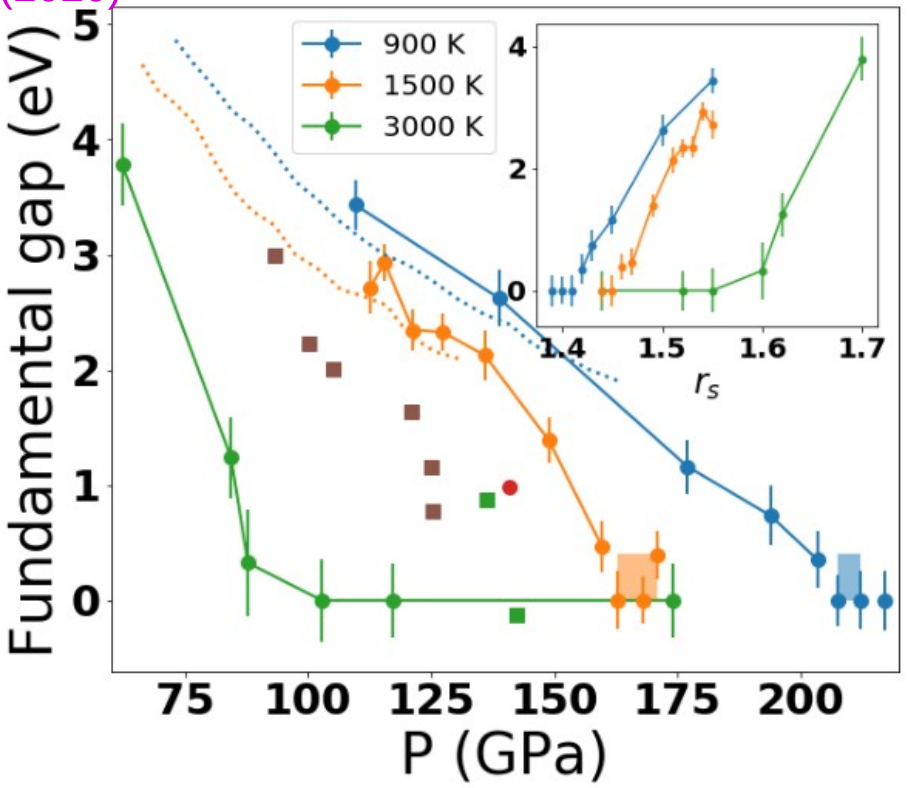

FIG. 31. The fundamental energy gap of liquid hydrogen along the isotherms: $T = 900\,\mathrm{K}$, $1500\,\mathrm{K}$ and $3000\,\mathrm{K}$, as a function of pressure. Inset: the same gap as a function of r_s, a measure of density, Eq. (1). The lines connect the gap data only up to the molecular-atomic transition region. The colored rectangles show the coexistence region of the LLPT according to Ref.[209]. The dotted lines are the gaps reported by P.M. Cellier *et al.*[234]. The brown and green squares are the results of W.J. Nellis *et al.* for temperatures of $2000\,\mathrm{K}\ldots 3000\,\mathrm{K}$[686] reanalyzed in Ref.[687]. The red dot is the gap reported by R.S. McWilliams *et al.* at $2400\,\mathrm{K}$[688]. Adapted from Ref.[510].

Fundamental (charged) and neutral gap In solid H_2 (phase I - HCP)

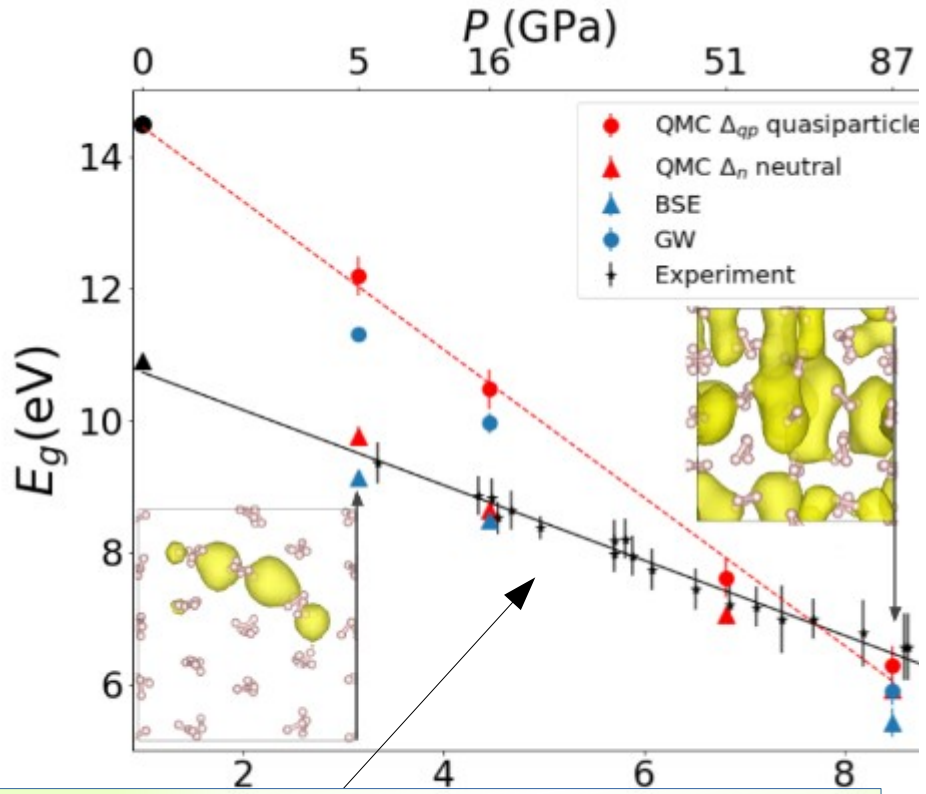

Experimental results from inelastic X-ray scattering:

Gap from lower limit of photon energy loss spectra

B. Li, Y. Ding, D. Y. Kim, L. Wang, T.-C. Weng, W. Yang, Z. Yu, C. Ji, J. Wang, J. Shu, J. Chen, K. Yang,Y. Xiao, P. Chow, G. Shen, W. L. Mao, H.-K. Mao, Phys. Rev. Lett. 126, 36402 (2021).

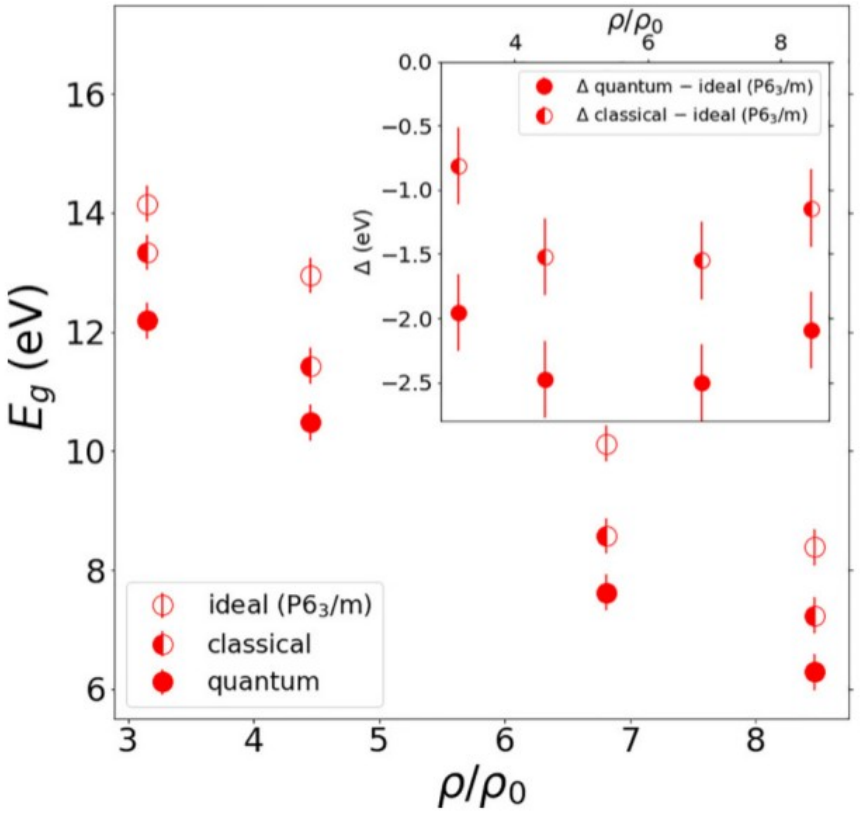

FIG. 4. Quasiparticle (QP) gap of the ideal $P6_3/m$ structure (open circles), QP gap with classical protons at room temperature (half circle), and QP gap with quantum protons at room temperature (solid circle). Inset: The reduction of the quasiparticle gap due to temperature and quantum nuclear effects (solid circles) and with only temperature effects (half-filled circles).

V. Gorelov, M.H., D.M. Ceperley, C. Pierleoni, Phys. Rev. B 109, L241111 (2024)

Summary - Conclusions:

- Improvement of ground state wave functions:
  iterated backflow, machine learned network ansätze...
- Jellium: many-body correlations supress polarization transition,
  true for all isotropic and spin-intependent interactions?
- Gaps: single particle and p-h excitations, size effects, S(k)….
- Fermi Liquid parameters: Z, m*

David Linteau
Giuseppe Carleo
(EPFL)

Saverio Moroni
(CNR, SISSA, Trieste)
Vitaly Gorelov
(Palaiseau)
Carlo Pierleoni
(University of L'Aquila)

Max Wilson
(DTU)

David Ceperley
(UIUC)
Ricky Niu
Scott Jensen
Paul Yang
Valerio Olevano
(Néel, Grenoble)